



Reinforced modified carboxymethyl cellulose films with graphene oxide/silver nanoparticles as antimicrobial agents

Hebat-Allah S. Tohamy*



Cellulose and Paper Department, National Research Centre, 33 El Bohouth Str., P.O. 12622, Dokki Giza, Egypt

Abstract

Ultra sonicated graphene oxide/silver nanoparticles (GO@ Ag⁰) which prepared by green chemistry approach in a microwave from sugarcane bagasse (SCB) were mixed with carboxymethyl cellulose (CMC) at varied loading ratios (5–15wt %) to create biopolymer films. The GO@ Ag⁰ forms a network with the CMC matrix, which was first proved by the MHBS calculations, SEM, thermal and mechanical data. This finding confirmed that the GO@Ag has high compatibility within the CMC matrix owing to the oxygenated graphene oxide (GO). Furthermore, with the addition of 15wt% GO@ Ag⁰ (i.e. CMC–GO@Ag 15%), 14.31% increase of thermal stability, 96.13% of YM, and 16.82% of TS were achieved. Moreover, the CMC–GO@Ag5%, CMC–GO@Ag10% and CMC–GO@Ag15% films exhibit greater efficacy against both Gram +ve and -ve bacteria as well as yeast compared to pristine CMC film. We might suppose that these films' outstanding performance made them suitable for food packaging (due to its anti-microbial properties) and electrochemical biosensing (due to the presence of Ag⁰).

Key words: Carboxymethyl cellulose; Graphene oxide/silver; Microwave; Antimicrobial agents; Agricultural wastes; Biopolymers; Films.

1. Introduction

Because of the environmental issues of the plastic industry, there is an importance of looking at sustainable packaging materials. The aim focuses on replacing out plastic based polymers to biodegradable ones (i.e. biopolymers) 1,2. Utilizing biopolymers has several benefits, including biodegradability, biocompatibility, low cost, and sustainability 3. The edible biopolymers are alternatives to plastics in food packaging applications. The edible films are made from polysaccharides such as carboxymethyl cellulose (CMC) 1. CMC is a characteristic polysaccharide prepared from the agricultural wastes such as sugarcane bagasse (SCB) by the mercerization of cellulose which extracted from SCB. Agricultural wastes are abundant, ecofriendly materials that can easily be recycled into valuable products. The primary component of these wastes is cellulose, which is made up of 1,4-glycosidic linkages of the D-glucose unit which can be modified to CMC 4. CMC is a hydrophilic form of cellulose which was better to be used in packaging applications

than other biopolymers such as methyl cellulose, gelatin, etc. due to its good film forming ability 1,4-6. The drawback is that the edible CMC matrix properties may not be the best and need more modifications to enhance the end use properties 7. To meet market needs, the edible films can be reinforced by suitable nanofillers such as graphene (G). This can be thought of as a trustworthy method to improve the mechanical and thermal features of the pristine biopolymer film. Graphene oxide (GO) has been used as a nanofiller instead of G due to its compatibility with organic biopolymers 2. It can be easily obtained by eco-friendly and attractive economical technique from SCB in a muffle furnace. GO is an oxygenated form of G with a superior surface area properties. This can enhance the dispersion of GO nanosheets and producing high interfacial interactions with the functional groups of hydrophilic biopolymers such as CMC matrix 2-4.

At the same time, food can become polluted while being stored, prepared, and transported. This will enhance food deterioration. Silver nanoparticles (Ag

*Corresponding author e-mail: hebasarhan89@yahoo.com; (Hebat-Allah S. Tohamy).

Receive Date: 22 August 2022, Revise Date: 20 September 2022, Accept Date: 02 October 2022

DOI: 10.21608/EJCHEM.2022.157801.6834

©2022 National Information and Documentation Center (NIDOC)

NPs), which are more efficient antimicrobial agents than other metallic NPs, can be incorporated into the film matrix to deal with this problem and promote microbiological safety and food preservation^{8,9}. Green synthesis approach of Ag NPs in a domestic microwave is considered more economical and eco-friendly approach as compared to classical techniques¹⁰.

Current research has focused on integrating AgNPs with another biocompatible polymer i.e., GO to produce microwave assisted in-situ GO@ Ag₀. This synthesized GO@ Ag₀ can be added to pristine CMC matrix to improve its antibacterial activity, thermal and mechanical properties. Additionally, these films can be used in our future researches in food and electronic packaging, as well as, electrochemical biosensing.

Experimental materials and devices:

Sugarcane bagasse (SCB) was obtained from Quena Company for Paper Industry (Egypt). All materials and reagents were applied without further purification.

Fourier-transform infrared spectra were performed employing Mattson 5000 spectrometer using the KBr disk method. The crystallinity was studied on X-ray powder diffraction as the diffraction patterns were measured by Bruker D-8 Advance X-ray diffractometer (Germany) applying a 40 kV voltage and a 40 mA current employing copper (K α) radiation (1.5406 Å) peak, respectively 6.

$$\text{Cr.I}(\%) = \frac{A_c}{A_t} \times 100 \quad (1)$$

$$\Delta \text{Cr.I}(\%) = \frac{(\text{Cr.I. of adjusted sample} - \text{Cr.I. of unadjusted sample})}{\text{Cr.I. of adjusted sample}} \times 100 \quad (2)$$

Where A_c = area of the crystalline domain, A_t = area of the total domain, Cr.I (%) = crystallinity index and $\Delta \text{Cr.I}(\%)$ = change of crystallinity⁶.

The d spacing (thickness) was calculated using Bragg's law and the crystallite size can be calculated by using Scherrer's equation^{4,6}. TGA analysis was performed on the prepared polymer powder employing Perkin Elmer thermogravimetric analyzer by heating the sample to 1000°C at a rate of 10°C/min under N₂ atmosphere. Kinetics of thermal decomposition was explored for pristine CMC film and CMC-GO@Ag 15% samples by Coats-Redfern approach. The enthalpy (ΔH), entropy (ΔS) and free energy change (ΔG) were also estimated eq. (3):

$$\Delta H^* = E^* - RT, \quad \Delta G^* = [\Delta H]^* - T\Delta S^* \quad \text{and}$$

$$\Delta S^* = 2.303(\log Ah/KT)R \quad (3)$$

where (h) and (k) are Planck and Boltzman constants, respectively 3,4,6.

The morphology of samples was performed by using scanning electron microscopy (SEM, Quanta-250). The mechanical properties were performed by using 'Universal Testing Machine' model 4201. Young's modulus (YM), tensile strength (TS) and elongation at break (EB) were estimated by visual examination of the film breakage from linearity of the plot. The antimicrobial activity was performed by the disc diffusion method. The inhibition zones were measured in millimeters.

Preparation of cellulose from sugarcane bagasse (SCB)

SCB was hydrolyzed with 1.5% HCl and 20% NaOH. Mercerization of cellulose was carried out by 17.5% NaOH to remove the traces of lignin and other constituents 4.

Synthesis of carboxymethyl cellulose (CMC)

A typical process involved adding a 30% NaOH solution dropwise for 30 min. to cellulose suspended in 400 ml isopropanol, followed by 1 hr of stirring at room temperature. Then, the mixture received dropwise additions of 18 g of mono chloroacetic acid (MCA) dissolved in isopropanol for 30 min. For 3.5 hrs, the mixture was allowed to react at 55 °C while being stirred. The fibrous result is mixed in 70% methanol, filtered, and dried at 60 °C. the produced CMC has a degree of substitution ~ 0.7 4.

Microwave in-situ preparation of GO embedded with silver (GO@Ag₀)

500 mg SCB and 100 mg ferrocene was placed into a muffle furnace at 300 °C for 10 min 3,4,6. The as-produced GO was mixed with 500 ppm AgNO₃ and subjected to ultra-sonication for 30 min. Then, it was put in a domestic microwave for 120 sec at 90 W. The obtained dry black powder is GO@ Ag₀ 10.

Preparation of CMC films embedded with GO@ Ag₀ (CMC-GO@Ag)

1 gm of CMC was dissolved in 20 ml H₂O and ultrasonicated with different ratios of GO@ Ag₀ i.e. 5, 10 and 15% which denoted as CMC-GO@Ag 5%, CMC-GO@Ag 10% and CMC-GO@Ag 15% and poured separately onto teflon plate and dried at 45°C to film of constant weight 11.

Results and discussion

FTIR spectroscopy

FT-IR spectrum of Cellulose and CMC reveals peaks centered between 3351-3361, 2879-2917,

1594-1643, 1417-1438, 1322-1332 and 105-1060 cm^{-1} which attributed to stretching vibration modes of OH, CH, C=O, O-C=O, C-O and C-O-C groups, respectively^{3,4}. While, GO@ Ag0 shows peaks at 3311, 2925, 1604, 1452, 1400 and 1076 cm^{-1} which attributed to stretching vibration modes of OH, CH, C=O, O-C=O, C-O and C-O-C groups, respectively⁶. As shown in Fig. 1, the FTIR spectra of CMC-GO@Ag 5%, CMC-GO@Ag 10% and CMC-GO@Ag 15% were similar to GO@ Ag0 with small band shift toward low wavenumbers (i.e. from 1594 to 1564, 1569 and 1575 cm^{-1}), which indicates the strong interaction operates between CMC and GO@ Ag0 through the formation of H-bond, $\pi \rightarrow \pi^*$ interaction or electrostatic attraction^{4,12}. H-bonded OH stretching vibration of CMC appeared at 3361 cm^{-1} was shifted to lower frequency at 3359, 3355 and 3349 cm^{-1} for CMC-GO@Ag 5%, CMC-GO@Ag 10% and CMC-GO@Ag 15%, respectively. The change of the absorbance value of OH stretching vibration may be due to intermolecular H-bonding. The relative absorbances (RAs) of the O-H were 0.99, 1.04, 0.98, 0.98 and 0.97 for pristine CMC matrix, GO@ Ag0, GO@Ag 5%, GO@Ag 10% and GO@Ag 15%, respectively. It is clear that the RAs of the O-H strongly decreased compared to that of pristine CMC film. This means that the cross-linking reaction took place between the OH group of pristine CMC film and GO@ Ag0^{4,6}. Measuring mean hydrogen bond strength (MHBS; AOH/ACH) revealed the higher values of CMC-GO@Ag 15% than other modified films. This may be due to the strong interaction between CMC matrix and GO@ Ag0.

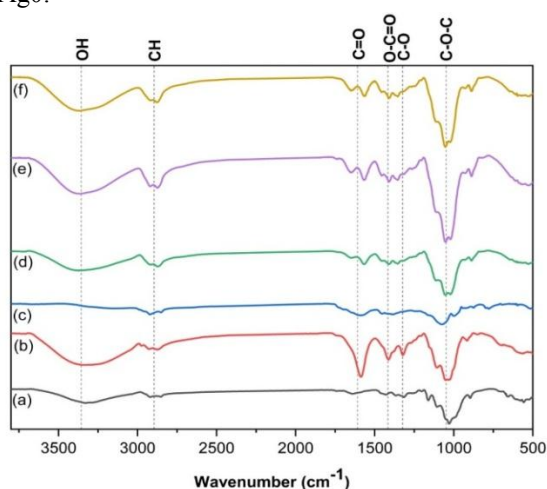


Figure 1: FTIR of (a) Cellulose, (b) pristine CMC film, (c) GO@Ag0, (d) CMC-GO@Ag 5%, (e) CMC-GO@Ag 10%, and (f) CMC-GO@Ag 15%.

Table 1: MHBS of cellulose, Pristine CMC film, GO@Ag0, CMC-GO@Ag 5%, CMC-GO@Ag 10% and CMC-GO@Ag 15%.

Sample	MHBS (AOH/ACH)
Cellulose	0.95
Pristine CMC film	0.91
GO@Ag ⁰	1.04
CMC-GO@Ag 5%	0.97
CMC-GO@Ag 10%	0.97
CMC-GO@Ag 15%	0.98

X-ray analysis

X-ray diffraction patterns of cellulose showed peaks at 11.45, 19.97 and 21.46 $^{\circ}$, the splitting in the reflection bands at 19.97 and 21.46 $^{\circ}$ correlated to (110), (110) and (020); which are related to the cellulose-II pattern. However, the XRD pattern of the neat CMC film indicates reflections at 13.29, 19.22 and 21.12 $^{\circ}$. The broadening of 19.22 and 21.12 $^{\circ}$ peaks indicates the amorphous structure of CMC^{4,6}. The GO@ Ag0 shows reflections at 9.03 and 21.20 $^{\circ}$ correlated to (001) and (002) plans of GO^{3,4,6,12-17}, as well as, the reflections at 27.94, 33.68, 44.66 and 47.04 $^{\circ}$ correlated to the (111), (200), (220) and (311) planes of face-centered-cubic Ag^{18,19}.

The modified samples (i.e. CMC-GO@Ag 5%, CMC-GO@Ag 10%, and CMC-GO@Ag 15%) have a broad diffraction peak at $2\theta = 7.06^{\circ}$, 9.00 and 10.00, as well as, other one at $2\theta = 21.24$, 21.62 and 22.00 $^{\circ}$ that are characteristic of GO@Ag0. The intensity of the peaks correlated to GO@Ag in CMC-GO@Ag 5% are very small due to the low concentration of it. The variations in the crystalline constitution of pristine CMC film, CMC-GO@Ag5%, CMC-GO@Ag10% and CMC-GO@Ag15% occur due to graft copolymerization on the CMC matrix.

The crystallinity indexes calculated for cellulose, pristine CMC film, GO@ Ag0, CMC-GO@Ag5%, CMC-GO@Ag10% and CMC-GO@Ag15% were 61.02, 46.16, 3.98, 5.01, 0.95 and 2.55%, respectively. It is clear that Cr.I (%) of modified films (i.e., CMC-GO@Ag5%, CMC-GO@Ag10% and CMC-GO@Ag15%) decreased, compared with that pristine CMC film and GO@Ag0. This may be due to the sonication process during the preparation. The XRD Cr.I (%) values didn't agree with the MHBS values calculated from the FIR spectra of cellulose. This may be due to the type of H-bonding (i.e., intra and inter H-bonding)^{3,4}. As shown in table 2, d (nm) of CMC-GO@Ag 15% is decreased compared to other modified films (i.e. CMC-GO@Ag 5% and CMC-GO@Ag 10%). This may be due to the strong

interaction between CMC matrix and GO@Ag which decrease the distance between them 4.

Table 2: Crystallinity, d and crystal size of Cellulose, pristine CMC film, GO@Ag⁰, CMC-GO@Ag 5%, CMC-GO@Ag 10%, and CMC-GO@Ag 15%.

Sample	Cr.I (%)	Δ Cr.I (%)	d (nm)	Crystal size (nm)
Cellulose	61.02	-	26.66	0.32
Pristine CMC film	46.16	-	16.58	3.55
GO@Ag ⁰	3.98	-1059.79	19.32	0.84
CMC-GO@Ag 5%	5.01	-821.35	32.59	1.18
CMC-GO@Ag 10%	0.95	-4758.94	27.59	1.00
CMC-GO@Ag 15%	2.55	-1710.19	23.22	0.48

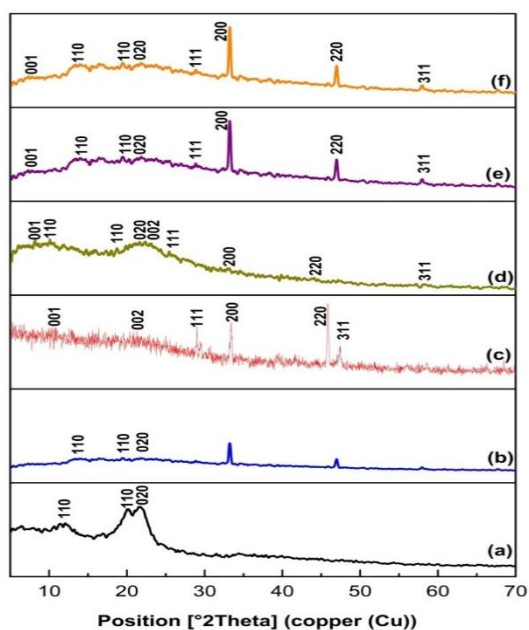


Figure 2. XRD analysis of (a) Cellulose, (b) Pristine CMC film, (c) GO@Ag⁰, (d) CMC-GO@Ag 5%, (e) CMC-GO@Ag 10%, and (f) CMC-GO@Ag 15%.

Morphological properties

Figure 3 shows the surface morphology of Cellulose, pristine CMC film, GO@Ag⁰ and CMC-GO@Ag15%, and how the modification process affected on CMC and GO@Ag⁰ surface morphology. The ordered structure of cellulose changed after mercerization and the formation of pristine CMC film. As it seems in Fig. 3a&b the rodlength was

decreased from 345.09 to 60.36 nm due to the backbone structure of cellulose is destroyed as a result of the ring-opened formation. The morphology of the synthesized GO@Ag⁰ is sheets randomly aggregated with rounded folds 4,6. In addition, the insertion of Ag NPs was occurred over the surface of GO (Fig. 3c) with the creation of porous structure (pore size ~ 68.31 nm) and the deposited glowy spots (particle size ~ 11.44 nm) on the surface of GO is observed due to formation of Ag⁰ through heating in the microwave. The prepared CMC-GO@Ag15% film was solid and the pores are hidden, which was explained by the fact that the GO@Ag⁰ aggregate when GO@Ag NPs loading became higher than 10%. The films porosity were calculated from the SEM figures and introduced in Table 3. The porosity and surface area of pristine CMC film was increased with addition of GO@Ag⁰ ~ 11.78 and 402.68 %, respectively, for CMC-GO@Ag 15% compared to pristine CMC film.

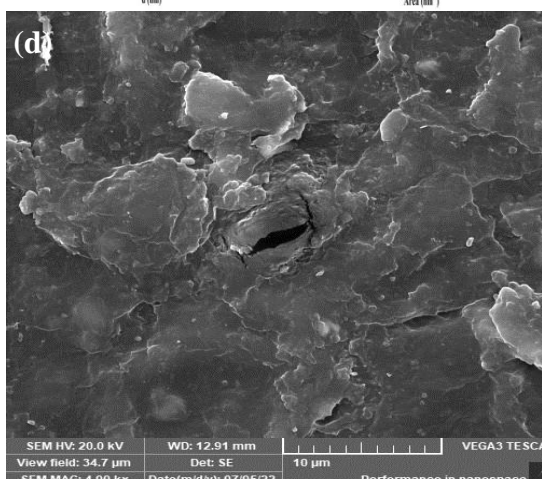
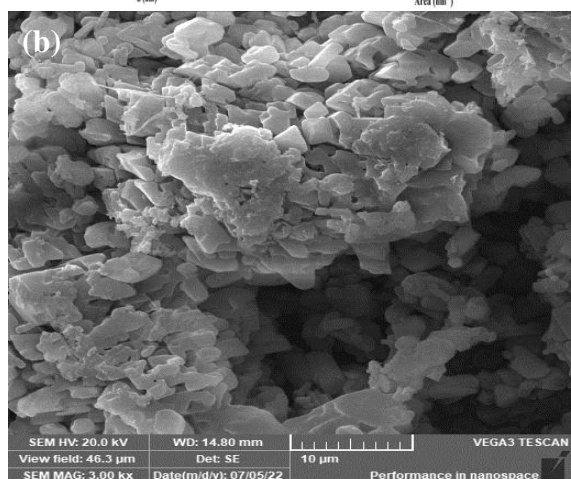
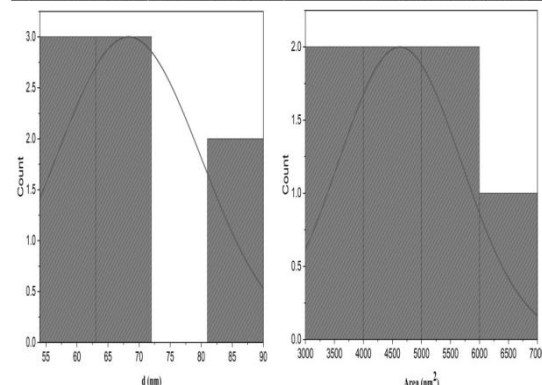
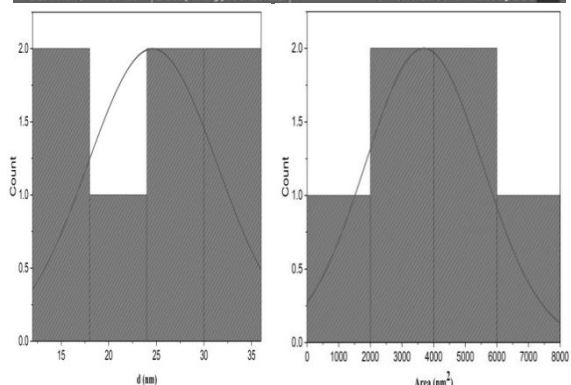
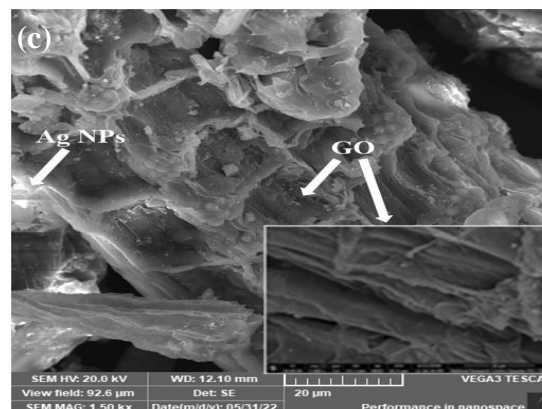
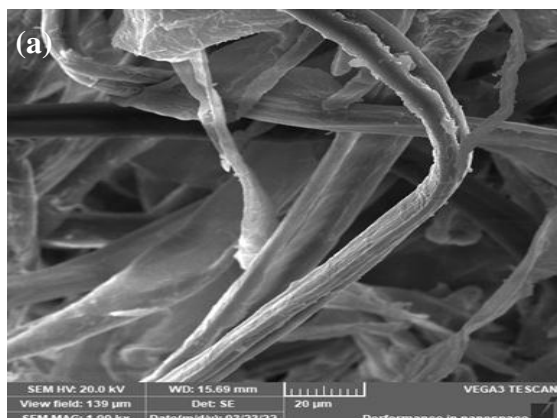
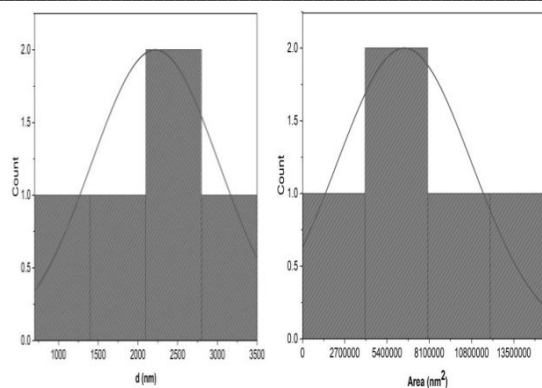
Thermal properties

The TGA/DTG of pristine CMC film blank and CMC-GO@Ag 15% showed a weight loss ~ 70.03 and 68.83%, respectively, at 1000°C, which indicated the presence of a fraction of non-volatile components. The thermal decomposition processes of CMC-GO@Ag15% could be divided into two major reaction steps, where the 1st weight loss was between 38.48-158.59°C, with a maximum ~ 99.31 °C and mass loss (ML %) ~ 4.88% because of the loss of moisture content. The main 2nd decomposition step was between 195.96-452.12°C, with a maximum ~ 338.08°C, $\sum E_a$ ~ 26.99 kJ/mole and ML ~ 63.95%, ascribed to the depolymerizations and carbonization 3,4,6,20.

Pristine CMC film could be divided into four major reaction steps, where the 1st decomposition step between 28.95-183.25°C, with a maximum ~ 122.52°C and ML ~ 4.88%, ascribed to the moisture content. The main 2nd and 3rd decomposition steps between 209.01-351.22 and 368.18-515.07°C with the total activation energy ($\sum E_a$) ~ 23.61 kJ/mole, ascribed to the dehydroxylation and pyrolytic fragmentation. The 4th decomposition step between 856.59-986.09°C, with a maximum ~ 923.10°C and ML ~ 5.19%, ascribed to the decomposition of the carbonaceous residues 3,4,20.

Table 3: Porosity (%), area (nm²) and pore size (nm) of cellulose, pristine CMC film, GO@Ag⁰ and CMC-GO@Ag 15%.

Sample	Porosity (%)	Area (nm ²)	Pore size (nm)
Cellulose	70.23	191.00	-
Pristine CMC film	59.49	24.60	515.06
GO@Ag ⁰	59.55	4627.71	68.31
GO@Ag 15%	66.44	123.66	11.21



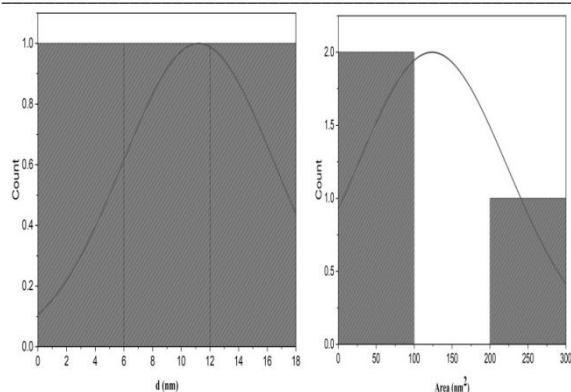


Figure 3. SEM analysis of (a) Cellulose, (b) pristine CMC film, (c) GO@Ag⁰, (d) CMC-GO@Ag 15%.

The increase in the maximum peak of the 1st stage for CMC-GO@Ag 15% compared to pristine CMC film indicating that the GO@Ag⁰ were evenly distributed throughout the CMC matrix, operating as an interconnected network within the CMC matrix and preventing the CMC-GO@Ag 15% film from absorbing water when exposed to moisture. Increasing in $\sum E_a$ of the 2nd main stage for CMC-GO@Ag 15% (26.99 kJ/mole) compared to the 2nd and 3rd main stages of pristine CMC film (23.61 kJ/mole), indicates thermal stabilization of CMC-GO@Ag 15%. Therefore, it requires high E_a to degrade. The residual weight (RW %) of CMC-GO@Ag 15% is higher than pristine CMC film which proves the thermal stability of CMC-GO@Ag 15%. This may be due to the adhesion between CMC chains and GO@Ag⁰. There is an agreement between the data of E_a and that of MHBS calculated from FTIR. But, there is no conformity with Cr.I (%) data which calculated from XRD. This may be due to the type and degree of H-bonding formed 4,6,20.

According to Table 3, all samples under investigation have values for ΔS that are negative, indicating that the system is becoming less disordered and that degradation won't happen naturally. The CMC-GO@Ag 15%'s high ΔS (-0.45 KJ mol⁻¹) indicates that its thermal degradation was more complex (requiring more time and external energy to breakdown) than the pristine CMC film (-0.95 KJ mol⁻¹) 21, 22. Additionally, the value of ΔH for the pristine CMC decreases from about -3.28, 59.01, and 45.83 kJ mol⁻¹ at the early stages of the reaction to about -9.94 kJ mol⁻¹ at the final stage, indicating a very low energy requirement as the reaction progresses. With lowering n (0.5) value, the ΔH was reduced (-9.94 kJ mol⁻¹). The pristine CMC film may be broken down with very little energy, according to this. The presence of activated carboxymethyl terminal groups, which are regarded as an excellent leaving group, can be responsible for the observable fall in H for the pristine CMC film. A decrease in H is also suggested by the CMC's bifunctionality (i.e., the presence of both COOH and OH groups), which has a strong probability of crosslinking. As the reaction progresses, a very minor change in the value of ΔH with respect to n and T is observed. At the start of the reaction, it was roughly 19.27 kJ mol⁻¹, and at its completion, it was roughly 20.62 kJ mol⁻¹. For the pristine CMC film and CMC-GO@Ag 15%, the G changes ranged within 91.61-285.90 and 107.07-180.68 kJ mol⁻¹, respectively. The CMC-GO@Ag 15% is more non spontaneous and requires external heat input than the pristine CMC film 22, according to the ΔG observations.

Table 3: TGA/DTG data of pristine CMC film and CMC-GO@Ag 15%

Sample	Stage	TGA range, °C	DTA peak, °C	Mass loss (%)	n	R^2	A (s ⁻¹)	ΔH (Kj mol ⁻¹)	Δs (Kj mol ⁻¹)	ΔG (Kj mol ⁻¹)	SE	E_a (kJ mol ⁻¹)
Pristine CMC film	1 st	28.95-183.25	122.52	4.88	0	0.9978	2.42	-3.28	-0.23	91.61	49X10 ⁻³	4.81
	2 nd	209.01-351.22	298.35	42.58	0.5	0.9987	2.84	59.01	-0.24	197.09	30X10 ⁻³	9.08
	3 rd	368.18-515.07	456.84	17.38	2.5	0.9997	4.28	45.83	-0.24	221.20	17X10 ⁻³	14.53
	4 th	856.59-986.09	923.10	5.19	0.5	0.9998	3.00	-9.94	-0.24	285.90	57X10 ⁻⁴	19.85
				$\sum ML=70.03$ $\sum RW=29.97$					$\sum S=-0.95$			$\sum E=49.08$
CMC-GO@Ag 15%	1 st	38.48-158.59	99.31	4.88	1.5	0.9390	3.74	19.27	-0.23	107.07	86X10 ⁻²	22.37
	2 nd	195.96-452.12	338.08	63.95	1.5	0.9721	0.26	20.62	-0.26	180.68	74X10 ⁻²	26.99
				$\sum ML=68.83$ $\sum RW=31.17$					$\sum S=-0.49$			$\sum E=49.36$

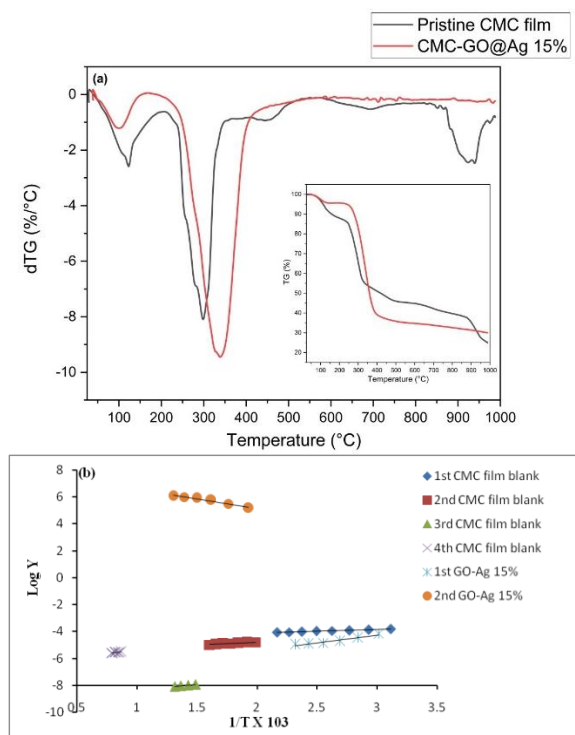


Figure 4.(a) TGA/DTG of pristine CMC film and CMC-GO@Ag15% & (b) kinetics of thermal analysis.

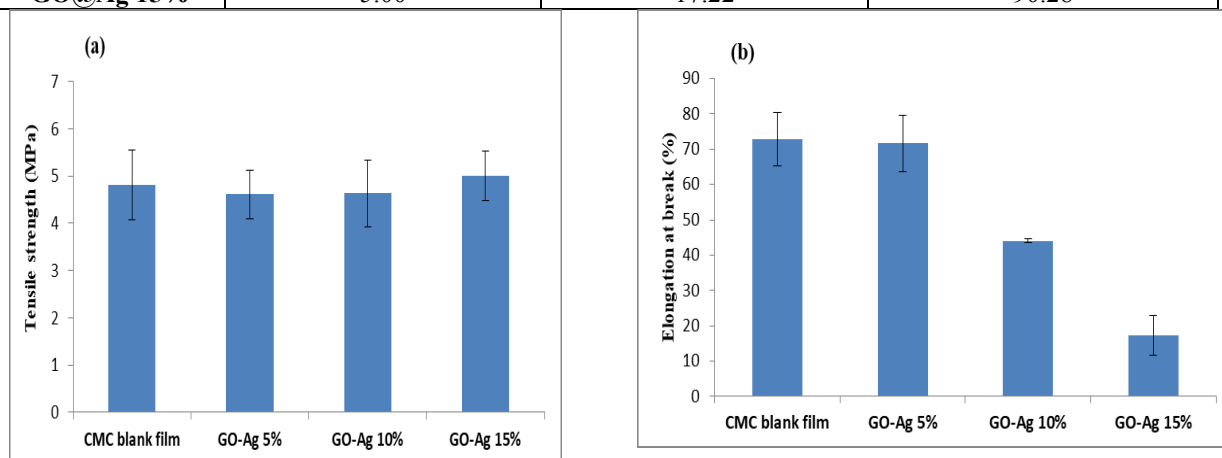
Mechanical properties

Tensile properties of pristine CMC blank film have been remarkably affected by adding varied GO@Ag0 concentrations. Mechanical properties of pristine CMC film, TS of 4.28 MPa and YM of 46.43

MPa, are significantly enhanced after adding GO@Ag0. For both low and high GO@Ag0 loadings, the addition of GO@Ag0 progressively enhanced the CMC matrix's chosen tensile characteristics. Upon addition of GO@Ag0; CMC-GO@Ag 15% tensile properties have been enhanced (TS of 5.00 MPa and YM of 90.28 MPa). There was conformity between the data of TS and thermal Ea calculated from TGA/DTG. This is an indication for the effect of GO@Ag0 on the elasticity of CMC films. Consequently, it is clear that the reinforcement efficiency of CMC-GO@Ag15%, at high loading level, is large superior than other ratios (i.e. CMC-GO@Ag 5% and CMC-GO@Ag 10%). The rigidity of CMC-GO@Ag 15% was increased and allowed less flexibility, which is good for the rigid packaging applications for fragile food products such as yogurt [2, 22, 23]. Regarding EB (%), it generally tended to decrease with addition of GO@Ag0. This may be due to the strong interaction between CMC matrix and GO@Ag0 which suppress the mobility of the CMC chains [2]. Comparing the improvement in TS and YM achieved in the current work to the aforementioned findings clearly shows the advantage of using reinforcement GO@Ag isolated from SCB pulp by direct microwave treatment.

Table 4: Mechanical properties of Pristine CMC film, CMC-GO@Ag 5%, CMC-GO@Ag 10% and CMC-GO@Ag15%.

Sample	Tensile strength (MPa)	Elongation at break (%)	Young's modulus (MPa)
CMC blank film	4.28	72.77	46.03
GO@Ag 5%	4.61	71.61	53.00
GO@Ag 10%	4.63	44.06	58.03
GO@Ag 15%	5.00	17.22	90.28



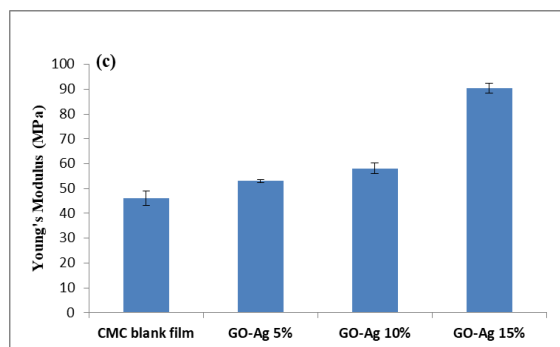


Figure 5. Mechanical properties of Pristine CMC film, CMC-GO@Ag 5%, CMC-GO@Ag 10% and CMC-GO@Ag15%.Anti-microbial activity

To promote the antimicrobial activity of pristine CMC film, it was supported with the GO@Ag which prepared from SCB to prepare CMC-GO@Ag5%, CMC-GO@Ag10% and CMC-GO@Ag15% films.

Table 5: Inhibition zones generated by Pristine CMC film, GO@Ag⁰, CMC-GO@Ag 5%, CMC-GO@Ag 10% and CMC-GO@Ag15%.

Sample <i>Test bacteria</i>	Gram -ve bacteria		Gram +ve bacteria		Pathogenic yeast
	<i>Escherichia coli</i>	<i>Pseudomonas aeruginosa</i>	<i>Micrococcus leutus</i>	<i>Staphylococcus aureus</i>	<i>Candida albicans</i>
Gentamicin	20.0	13.0	25.0	18.0	-
Miconazole	-	-	-	-	11.0
Pristine CMC film	19.0	Nil	Nil	Nil	20.0
GO@Ag ⁰	22.0	20.0	24.0	13.0	Nil
GO-Ag 5%	22.0	19.0	12.0	17.0	17.0
GO-Ag 10%	35.0	31.0	31.0	22.0	22.0
GO-Ag 15%	22.0	22.0	30.0	21.0	21.0



The samples' antimicrobial efficacy was examined against *Escherichia coli*, *Pseudomonas aeruginosa*, *Micrococcus leutus*, *Staphylococcus aureus* and *Candida albicans*. Table 5 displays the inhibitory zones measurements (mm) in comparison to the generated one by gentamicin and miconazole. The CMC-GO@Ag5%, CMC-GO@Ag10% and CMC-GO@Ag15% films exhibit greater efficacy against both Gram +ve and -ve bacteria as well as yeast compared to pristine CMC film. On the other hand, GO@Ag0only possesses antibacterial efficacy against *Escherichia coli* and *Candida albicans*. As can be seen in Table 5, CMC-GO@Ag15% causes greater inhibitory zones than gentamicin and miconazole.

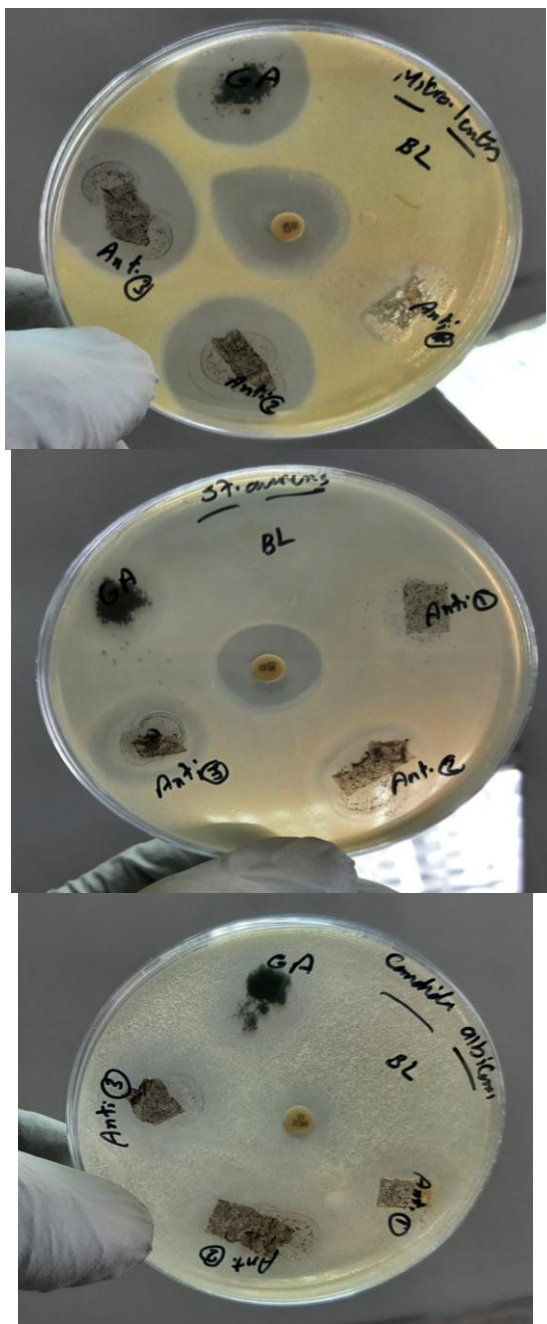


Figure 6. Inhibition zones generated by Pristine CMC film (denoted as BL), GO@Ag⁰ (denoted as GA), CMC-GO@Ag 5% (denoted as Anti 1), CMC-GO@Ag 10% (denoted as Anti 2) and CMC-GO@Ag15% (denoted as Anti 3).

Conclusion

To develop antibacterial, mechanical, and thermally stable films, GO@Ag⁰, which was synthesised using a green method, was dispersed into CMC biopolymer with a range of concentration ratios (5, 10 and 15wt%). It is proved that CMC matrix acquired strength by adding GO@Ag⁰ ratios as an interconnected framework. With addition of 15wt %

GO@Ag⁰ (i.e. CMC-GO@Ag 15%), 14.31 % increase of thermal stability, 96.13 % of YM, and 16.82% of TS were achieved. Moreover, the CMC-GO@Ag5%, CMC-GO@Ag10% and CMC-GO@Ag15% films exhibit greater efficacy against both Gram +ve and -ve bacteria as well as yeast compared to pristine CMC film. From these findings, we can say that the prepared CMC-GO@Ag 15% has combined between the properties of edible, eco-friendly films, tough, thermal stability and antimicrobial. So, these films have the capability to be used as packaging materials.

Conflict of interest

There are no conflicts to declare.

Acknowledgment

The author acknowledges the National Research Centre and the Academy of Scientific Research and Technology (ASRT), Egypt and Czech Academy of Sciences, for financial support of the bilateral research activities.

References

- 1 Al-Tayyar, N. A., Youssef, A. M., Al-Hindi, R. R. & Life, S. Antimicrobial packaging efficiency of ZnO-SiO₂ nanocomposites infused into PVA/CS film for enhancing the shelf life of food products. *J Food Packaging* 25, 100523 (2020).
- 2 El Achaby, M. et al. Mechanically strong nanocomposite films based on highly filled carboxymethyl cellulose with graphene oxide. *Journal of Applied Polymer Science* 133 (2016).
- 3 Tohamy, H.-A. S., El-Sakhawy, M. & Kamel, S. Development of graphene oxide-based styrene/acrylic elastomeric disks from sugarcane bagasse as adsorbents of Nickel (II) ions. *Journal of Polymer Research* 29, 1-13 (2022).
- 4 Tohamy, H.-A. S., El-Sakhawy, M. & Kamel, S. Development of Magnetite/Graphene Oxide Hydrogels from Agricultural Wastes for Water Treatment. *Journal of Renewable Materials* 10, 1889 (2022).
- 5 Choi, I. et al. Development of biopolymer composite films using a microfluidization technique for carboxymethylcellulose and apple skin particles. *International journal of molecular sciences* 18, 1278 (2017).
- 6 Tohamy, H.-A. S., Kamel, S. & El-Sakhawy, M. graphene oxide functionalized by ethylene diamine tetra-acetic acid (edta) by a hydrothermal process as an adsorbent for nickel ions. *Cellulose Chemistry & Technology* 55, 417-432 (2021).

- 7 Biswas, A. et al. Preparation and characterization of carboxymethyl cellulose films with embedded essential oils. *J. Mater. Sci. Res*7, 16 (2018).
- 8 Al-Tayyar, N. A., Youssef, A. M. & Al-Hindi, R. Antimicrobial food packaging based on sustainable Bio-based materials for reducing foodborne Pathogens: A review. *J Food chemistry*310, 125915 (2020).
- 9 Youssef, A. M., El-Sayed, S. M., El-Sayed, H. S., Salama, H. H. & Dufresne, A. Enhancement of Egyptian soft white cheese shelf life using a novel chitosan/carboxymethyl cellulose/zinc oxide bionanocomposite film. *J Carbohydrate Polymers*151, 9-19 (2016).
- 10 Rehan, M., Nada, A. A., Khattab, T. A., Abdelwahed, N. A. & Abou El-Kheir, A. A. Development of multifunctional polyacrylonitrile/silver nanocomposite films: Antimicrobial activity, catalytic activity, electrical conductivity, UV protection and SERS-active sensor. *Journal of Materials Research Technology*9, 9380-9394 (2020).
- 11 Krizova, H. & Wiener, J. Development of carboxymethyl cellulose/polyphenols gels for textile applications. *J Autex Res. J*13, 33-36 (2013).
- 12 Gordani, G. R., Estarki, M. R. L., Kiani, E., & Torkian, S. The effects of strontium ferrite micro- and nanoparticles on the microstructure, phase, magnetic properties, and electromagnetic waves absorption of graphene oxide-SrFe₁₂O₁₉-SiC aerogel nanocomposite. *Journal of Magnetism and Magnetic Materials*, 545, 168667 (2022).
- 13 Gordani, G. R., Estarki, M. R. L., Danesh, M., Kiani, E., & Tavooosi, M. Microstructure, phase, magnetic properties, and electromagnetic wave absorption of graphene oxide-Ni_{0.7}Zn_{0.3}Fe₂O₄-Al₂O₃ aerogel. *Ceramics International*, 48(3), 3059-3069 (2022).
- 14 Darwish, A., Ghoniem, A., Hassaan, M. Y., El-Said Shehata, O., & Turky, G. Synthesis and Characterization of Polyaniline/Mn₃O₄/Reduced Graphene Oxide Nanocomposite. *egyptian Journal of Chemistry*, 62(Special Issue (Part 1) Innovation in Chemistry), 251-265 (2019).
- 15 Rady, H., & Najim, S. Synthesize and Characterization of a Novel Nano Graphene Oxide Sulfolene derive. *Egyptian Journal of Chemistry*, 64(7), 3215-3223 (2021).
- 16 Mizhir, A., Abdulwahid, A., & Al-Lami, H. Chemical functionalization graphene oxide for the adsorption behavior of bismarck brown dye from aqueous solutions. *Egyptian Journal of Chemistry*, 63(5), 1679-1696 (2020).
- 17 Batiha, M. A., Dardir, M. M., Abuseda, H., Negm, N. A., & Ahmed, H. E. (2021). Improving the performance of water-based drilling fluid using amino acid-modified graphene oxide nanocomposite as a promising additive. *Egyptian Journal of Chemistry*, 64(4), 1799-1806 (2021).
- 18 Sajjad, M., Ahmad, F., Shah, L. A. & Khan, M. Designing graphene oxide/silver nanoparticles based nanocomposites by energy efficient green chemistry approach and their physicochemical characterization. *J Materials Science Engineering: B*284, 115899 (2022).
- 19 Rehan, M., Elshemy, N. S., Haggag, K., Montaser, A. & Ibrahim, G. E. Phytochemicals and volatile compounds of peanut red skin extract: Simultaneous coloration and in situ synthesis of silver nanoparticles for multifunctional viscose fibers. *Cellulose*27, 9893-9912 (2020).
- 20 Tohamy, H. A. S., Kamel, S., El-Sakhawy, M., Youssef, M. A., Abdallah, A. E., & Anis, B. Thermal properties of graphene oxide prepared from different agricultural wastes. *Egyptian Journal of Chemistry*, 63(10), 3619-3629 (2020).
- 21 Ivanovski, M., Petrovic, A., Ban, I., Goricanec, D., & Urbancl, D. Determination of the Kinetics and Thermodynamic Parameters of Lignocellulosic Biomass Subjected to the Torrefaction Process. *Materials*, 14(24), 7877 (2021).
- 22 Joraid, A. A., Okasha, R. M., Al-Maghrabi, M. A., Afifi, T. H., Agatemor, C., & Abd-El-Aziz, A. S. Thermodynamic Parameters of Non-isothermal Degradation of a New Family of Organometallic Dendrimer with Isoconversional Methods. *Journal of Inorganic and Organometallic Polymers and Materials*, 1-11 (2022).
- 23 Sennan, P. & Pumchusak, J. Improvement of mechanical properties of poly (lactic acid) by elastomer. *The Malaysian Journal of Analytical Sciences*18, 669-675 (2014).